

Article

Water/N,N-Dimethylacetamide-Based Hybrid Electrolyte and Its Application to Enhanced Voltage Electrochemical Capacitors

Aleksandra A. Mroziewicz ¹, Karolina Solska ¹, Grażyna Zofia Żukowska ² and Magdalena Skunik-Nuckowska ^{1,*}

¹ Faculty of Chemistry, University of Warsaw, Pasteura 1, 02-093 Warsaw, Poland; a.mroziewicz2@student.uw.edu.pl (A.A.M.); k.solska@student.uw.edu.pl (K.S.)

² Faculty of Chemistry, Warsaw University of Technology, Noakowskiego 3, 00-664 Warsaw, Poland; grazyna.zukowska@pw.edu.pl

* Correspondence: mskunik@chem.uw.edu.pl; Tel.: +48-22-55-26336

Abstract: The growing interest in hybrid (aqueous–organic) electrolytes for electrochemical energy storage is due to their wide stability window, improved safety, and ease of assembly that does not require a moisture-free atmosphere. When it comes to applications in electrochemical capacitors, hybrid electrolytes are expected to fill the gap between high-voltage organic systems and their high discharge rate aqueous counterparts. This article discusses the potential applicability of aqueous–organic electrolytes utilizing water/N,N-dimethylacetamide (DMAc) solvent mixture, and sodium perchlorate as a source of charge carriers. The hydrogen bond formation between H₂O and DMAc (mole fraction $x_{\text{DMAc}} = 0.16$) is shown to regulate the original water and cation solvation structure, thus reducing the electrochemical activity of the primary aqueous solution both in the hydrogen (HER) and oxygen (OER) evolution reactions region. As a result, an electrochemical stability window of 3.0 V can be achieved on titanium electrodes while providing reasonable ionic conductivity of 39 mS cm⁻¹ along with the electrolyte’s flame retardant and anti-freezing properties. Based on the diagnostic electrochemical studies, the operation conditions for carbon/carbon capacitors have been carefully optimized to adjust the potential ranges of the individual electrodes to the electrochemical stability region. The system with the appropriate electrode mass ratio ($m_+/m_- = 1.51$) was characterized by a wide operating voltage of 2.0 V, gravimetric energy of 13.2 Wh kg⁻¹, and practically a 100% capacitance retention after 10,000 charge–discharge cycles. This translates to a significant rise in the maximum energy of 76% when compared to the aqueous counterpart. Additionally, reasonable charge–discharge rates and anti-freeze properties of the developed electrolyte enable application in a broad temperature range down to –20 °C, which is demonstrated as well.

Keywords: double-layer electrochemical capacitor; N,N-dimethylacetamide; aqueous–organic solvent; hybrid electrolyte; hydrogen bond; hydrogen evolution reaction (HER)



Citation: Mroziewicz, A.A.; Solska, K.; Żukowska, G.Z.; Skunik-Nuckowska, M. Water/N,N-Dimethylacetamide-Based Hybrid Electrolyte and Its Application to Enhanced Voltage Electrochemical Capacitors. *Batteries* **2024**, *10*, 213. <https://doi.org/10.3390/batteries10060213>

Academic Editor: Douglas Ivey

Received: 17 May 2024

Revised: 6 June 2024

Accepted: 13 June 2024

Published: 19 June 2024



Copyright: © 2024 by the authors. Licensee MDPI, Basel, Switzerland. This article is an open access article distributed under the terms and conditions of the Creative Commons Attribution (CC BY) license (<https://creativecommons.org/licenses/by/4.0/>).

1. Introduction

Energy and power density are the two fundamental parameters describing electrochemical power sources. High power is an inherent feature of electrochemical double-layer capacitors (EDLCs) and is associated with operation mechanisms based on electrostatic (coulombic) interactions of ions with porous carbon electrode surfaces [1–3]. EDLCs, however, store much less energy than classical batteries, and although it is again an inherent property related to the storage mechanism, there is a growing number of studies aimed at searching for energy-enhancement strategies. Having in mind that the energy of a capacitor is expressed as $E = 1/2CU^2$, to boost the performance, one can either increase C (capacitance), U (the maximum voltage), or both, which is possible by manipulating the cell components, i.e., either the electrode material type and design on a molecular level or the electrolyte [3]. Intentional mass balancing, i.e., introducing an appropriate positive-to-negative electrode mass ratio helps to optimize the system as well [1,4].

The commercial market is dominated by EDLCs based on quaternary ammonium salts and organic solvents such as acetonitrile or propylene carbonate. Indeed, it is hard to compete with systems offering voltage of 2.7–2.8 V, which translates to gravimetric energies >20–30 Wh kg⁻¹ [1,3]. However, due to safety and economic concerns, numerous attempts have been made to design flammability issues-free, purely anhydrous electrolytes with high energy performance. In this respect, room-temperature ion liquids (ILs) and deep eutectic solvents (DES) should be mentioned as green and sustainable alternatives [5–7]. In practice, however, very low conductivity and high viscosity are serious limitation issues, especially considering low-temperature applications.

For many years, water-based electrolytes could not compete with organic solvent-based systems due to the narrow electrochemical stability window (ESW) of water, which, according to thermodynamic considerations, is equal to only 1.23 V. In practice, however, the cell potential in acidic and alkaline electrolytes is even more limited, i.e., up to 0.7–1 V [1,8,9]. Therefore, elaborating salt-in-water (SIW) [10–14] and water-in-salt (WIS) [15–20] strategies was an important breakthrough, especially when it comes to performance improvement of the EDL class of devices. SIW is an aqueous alkali metal salt-based electrolyte with a neutral pH. Due to the sluggish kinetics of water dissociation in neutral media and the fact that carbon electrode materials are rather poor at converting H adsorbates into gaseous H₂ under such conditions, the overpotential of the hydrogen evolution reaction (HER) is very high. As a result, the cell voltage can be expanded up to 1.5–1.6 V [13,14]. On the other hand, the WIS concept relies on highly concentrated (up to 21 mol kg⁻¹) aqueous salt electrolytes [15]. As demonstrated, when a solute's mass and volume are greater than the solvent's, almost all water molecules are bonded in the cation solvation shell, reducing water's chemical activity, and solvent splitting is highly suppressed [15,16]. As a result, the cell voltage of such an aqueous capacitor may easily exceed 2.0 V [16]. Such super-concentrated solutions may, however, suffer from limited ionic conductivity and elevated viscosity. The larger weight of the device is also an issue.

In this respect, aqueous–organic binary mixtures (hybrid electrolytes) can be considered an interesting alternative for WIS and SIW electrolytes [21–28]. Among important issues, their moisture-tolerant and non-flammable nature, as well as good wettability toward hydrophobic carbonaceous electrodes, should be mentioned. Additionally, the anti-freezing properties of some of the aqueous–organic mixtures may enable the operation of a capacitor at subzero temperatures. i.e., non-reachable for WIS and SIW electrolytes. To date, the co-solvent addition was considered to boost the performance of WIS systems in terms of transport properties and freezing temperatures while maintaining the elevated operating voltage. For instance, the addition of co-solvents such as acetonitrile (ACN), dimethyl carbonate (DMC), and dimethylformamide (DMF) have been studied in LiTFSI-based WIS systems [22]. A WIS/ACN (also known as AWIS) combination in the presence of less expensive NaClO₄ salt was also used to elevate the charge storage and rate capabilities of conventional WIS electrolytes [24,27]. Dimethyl sulfoxide (DMSO) is another example of a co-solvent used to design hybrid electrolytes for applications in batteries [29–31] and supercapacitors [25,26]. Its ability to partially replace H₂O molecules in the cation solvation shells and to form intermolecular hydrogen bonds with water results in significant suppression of the hydrogen evolution reaction (HER). As a result, an operating voltage reaching 2.0–2.1 V can be easily achieved for carbon/carbon capacitive cells with good cyclic performance.

Herein, we present another approach to design a hybrid aqueous–organic electrolyte based on water, acting as a hydrogen bond donor (HBA_d) and N,N-dimethylacetamide (DMAc) as hydrogen bond acceptor (HBD) to modify the water structure and, thus, to reduce its electrochemical activity. DMAc is a low-viscous and high boiling point polar aprotic solvent that is well-miscible with water. Its high dielectric constant of 37.8 and elevated flash point (when compared with ACN) make it a flame-retardant high-safety level electrolyte component. The physicochemical properties of moderately concentrated NaClO₄-based electrolytes in a mixed H₂O/DMAc solvent are discussed here and com-

pared to the purely aqueous and purely organic counterparts. The interactions between hydroxyl groups of water and carbonyl of amide, as well as the changes in the solvation structure, are documented based on the FTIR, Raman, and ^{23}Na NMR spectroscopies whilst the influence of the hydrogen bond formation on the ESW is independently studied using bare current collectors and activated carbon electrodes within the three-electrode setups. Based on the results, the complete two-electrode cells are built. Their performance is compared in symmetric ($m_+/m_- = 1$) and asymmetric ($m_+/m_- > 1$) configurations, where m_+ and m_- correspond to the mass of the positive, and the negative electrode, respectively. The electrical parameters are compared with those characteristics of the purely aqueous electrolyte-based cells.

2. Experimental

2.1. Materials and Preparation Methods

$\text{N,N-dimethylacetamide}$ (DMAc, 99.5%), sodium perchlorate monohydrate ($\text{NaClO}_4 \cdot \text{H}_2\text{O}$, 99.99%), and PTFE (60% aqueous dispersion) were purchased from Sigma Aldrich. Activated carbon powder (AC, YP, 80F), activated carbon cloth (ACC, 5092-20), and carbon black (C-nergyTM, Super C65) were from Kuraray (Tokyo, Japan), Kynol (Hamburg, Germany), and Imerys Group (Paris, France), respectively. The electrolytes were prepared by dissolving NaClO_4 in distilled water, DMAc, or a mixture of both solvents to result in 50% (*v/v*) DMAc, which corresponds to a mole fraction (x_{DMAc}) of 0.16. The molar concentration of salt in each electrolyte was equal to 1.73 mol dm^{-3} . The electrolytes were further denoted as H_2O , DMAc, and $\text{H}_2\text{O}/\text{DMAc}$. The electrodes for electrochemical tests were prepared by roll-pressing the mixture composed of 90 wt% AC, 5 wt% carbon black, and 5 wt % PTFE and then drying in the vacuum oven at 120°C before use. Before pressing, all constituents were homogenized in ethanol using a high-speed homogenizer (Vevor, Shanghai, China) at 20,000 rpm, followed by grinding in an agate mortar until the solvent was evaporated. The final thickness and surface area of the produced electrodes were $150 \pm 10 \mu\text{m}$ and $0.2826\text{--}0.785 \text{ cm}^2$ (diameter 6–10 mm) in all electrochemical cells. The mass of the individual electrodes (including binder and conductive additive) in symmetric systems and the three-electrode configuration diagnostic studies ranged from 5.6 to 5.9 mg (diameter 10 mm). The average mass loading in both electrodes was equal to 11.5 and 9.1 mg in all symmetric and asymmetric two-electrode cells, respectively. Celgard[®] 3501 (Charlotte, NC, USA) polypropylene film served as a separator.

2.2. Characterization Methods

The electrochemical stability window (ESW) of the electrolytes was determined in a glass cell equipped with a titanium (Ti Grade 2) rod (surface area exposed to electrolyte equal to 0.2826 mm^2) as a working electrode, platinum coil counter electrode ($A = 3.6 \text{ cm}^2$, Lambda System, Warsaw, Poland) and saturated calomel reference electrode (SCE) (Lambda System). In the presence of activated carbon, the ESW was measured in three-electrode PFA Swagelok[®] cells (Swagelok, OH, USA) using AC (diameter 10 mm, thickness 150 μm) mass oversized ACC (diameter 10 mm, thickness 490 μm), and SCE as the working, counter, and reference electrodes, respectively. Two-electrode Swagelok[®] housings served for the characterization of the complete capacitors. Ti (Grade 2) rods (diameter 12.7 mm) each time served as blocking electrodes and current collectors. Before assembly, the electrodes were immersed in 10 mL of electrolyte and shaken using IKA KS130 laboratory shaker (Staufen, Germany) for 15 min. Electrochemical data was gathered using EC-Lab software (V11.27) of the Biologic VMP3 workstation using linear sweep voltammetry (LSV), cyclic voltammetry (CV), galvanostatic charge–discharge (GCD) at specific currents ranging from 0.1 to 10 A g^{-1} , and electrochemical impedance spectroscopy (EIS) at 0 V DC bias with sinus amplitude of 0.01 V over the frequency range between 0.005 Hz and 1 MHz. Except for the temperature measurements conducted in a climate chamber, all electrochemical experiments were performed at RT ($24 \pm 1^\circ\text{C}$). The electrical parameters were normalized per total mass of both electrodes.

The conductivity and pH of electrolytes were determined using a Metler Toledo (Greifensee, Switzerland) conductivity meter (Seven2Go S7) and a pH meter (FiveGo F2), respectively. Viscosity was measured using an IKA (Staufen, Germany) Rotavisc viscometer. Temperature-dependent parameters were determined in a double-jacket vessel connected to a bath circulator (IKA, Staufen, Germany) from 80 down to 0 °C. The lowest temperature limit was due to the apparatus's limitations. A contact angle goniometer (Ossila, Sheffield, UK) equipped with a digital camera was used for wettability measurements. A drop volume was equal to 7 µL. A polynomial fitting was applied to the edge of the droplet to determine the static contact angles. The thermal images were taken using a Uni-T 260B thermal imaging camera (Uni-Trend Technology, Dongguan, China). For the determination of SET (the self-extinguishing time), 0.5 mL of the solution was placed in a stainless steel bowl (diameter of 2 cm) and a fire gun was approached for 5 s to allow ignition. The sample burning time after removal of the fire gun was measured for the three independent samples and the average value was taken as the SET (s g⁻¹).

Raman spectra were gathered using a Nicolet Almega dispersive Raman spectrometer (Thermo Fisher Scientific, Waltham, MA, USA) and a high-resolution grating (2400 lines/nm) with a 532 nm excitation line at 100% laser power. The exposure time was set to 15 s (number of exposures: 2). FTIR spectra were recorded using a Thermo Nicolet Avatar 370 instrument (Thermo Fisher Scientific, Waltham, MA, USA) equipped with an ATR accessory (Thermo Fisher Scientific) with a diamond crystal plate. Each spectrum was averaged over 64 scans, and the wavenumber resolution was equal to 2 s⁻¹. ²³Na NMR spectra were recorded using a 300 MHz Bruker Advance III HD spectrometer. The chemical shifts were referenced to the external standard (0.1 mol dm⁻³ NaCl).

3. Results and Discussion

3.1. Physicochemical Properties of Electrolytes

Table 1 gathers the main physical properties of the constituents of the electrolytes (Figure 1a) [32–34]. Considering ACN as a standard electrolyte for organic EDLCs and also an additive for WIS electrolytes, some benefits of DMAc can be pointed out, especially including the elevated flash (63 °C vs. 2 °C for ACN) and boiling points (165 °C vs. 82 °C for ACN). Hence, DMAc is classified as a combustible liquid of Class III (National Fire Protection Association, NFPA) or a flammable but of a lower concern (Globally Harmonized System, GHS). Also, both solvents have almost identical dielectric constants (37.78 vs. 37.50 for ACN) and a low viscosity. The latter is higher for DMAc (0.89 mPa s vs. 0.33 mPa s for ACN) but similar to water (0.998 mPa s) and much lower than for propylene carbonate (2.4 mPa s), a widely used alternative for ACN in organic EDLCs. It is worth mentioning that the solvent's dielectric constant (ϵ) is inversely proportional to the interaction energy between ions with the opposite charge and, consequently, the ability of ion-pairs formation [35]. For the solvents with lower ϵ , the ion-pairing in the solution is privileged. Although the ϵ for H₂O/DMAc solvent mixtures has not been measured in the course of the study, a value >60 can be expected for this particular composition ($x_{\text{IDMAc}} = 0.16$) based on the literature reports providing better ion dissociation and less ion association in comparison to the purely organic solvent [34].

Table 1. The physical properties of solvents.

Solvent	Molar Mass (g mol ⁻¹)	Density * (g cm ⁻³)	Dielectric Constant *	Viscosity * (mPa s)	Boling Point (°C)	Flash Point (°C)
H ₂ O	18.01	0.997	78.30	0.89	100	-
DMAc	87.12	0.937	37.76	0.92	165	63

* at 25.0 °C.

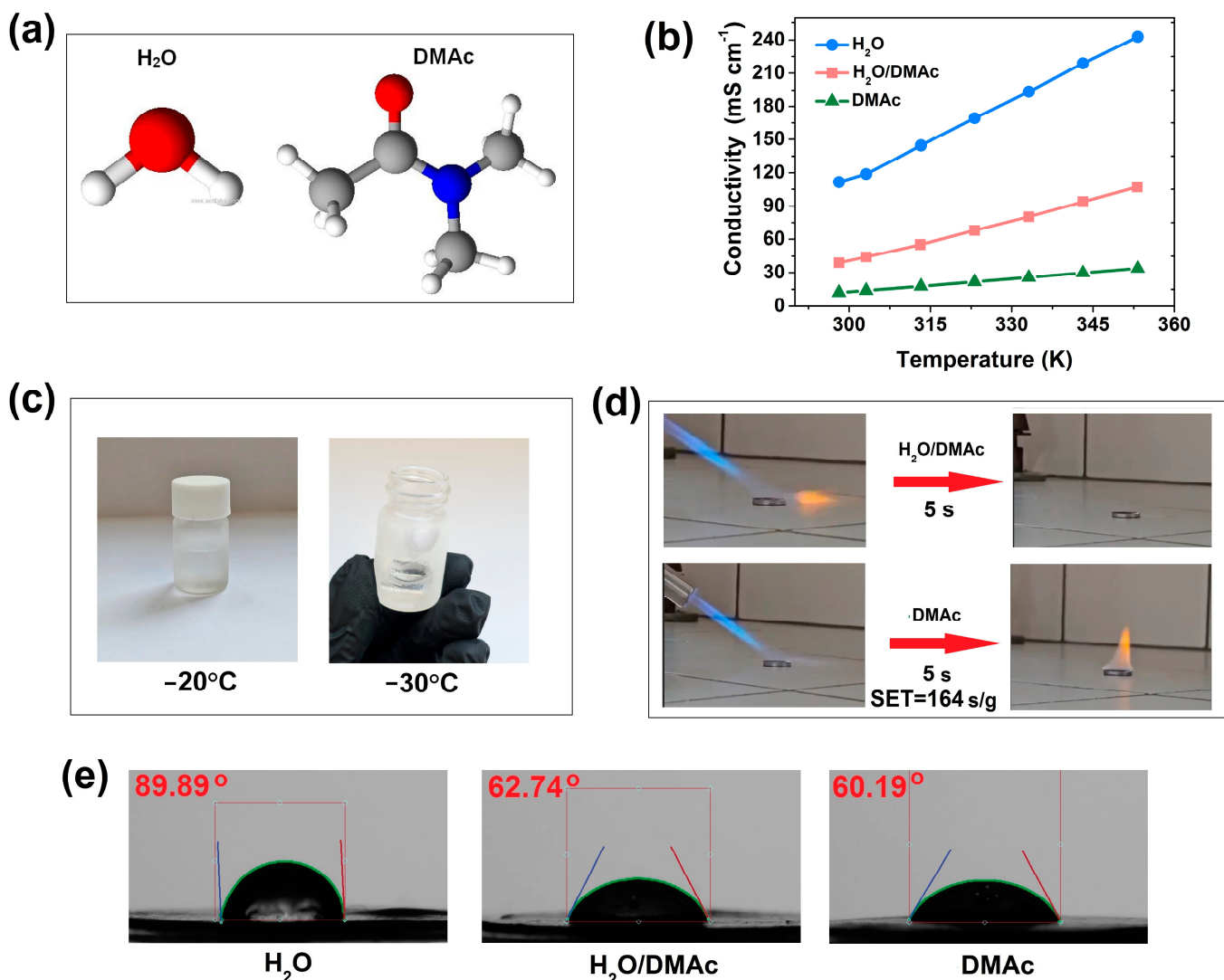


Figure 1. (a) Components of electrolyte and their chemical structure; (b) ionic conductivity as a function of temperature for NaClO_4 -based aqueous (H_2O), aqueous–organic ($\text{H}_2\text{O}/\text{DMAc}$), and organic (DMAc) solutions; (c) $\text{H}_2\text{O}/\text{DMAc}$ electrolyte at -20 and -30°C showing no sign of freezing; (d) comparative flammability tests for aqueous–organic and organic electrolytes; (e) static contact angles tests conducted at the surface of the AC electrode.

A higher degree of dissociation is expected to improve the ionic conductivity of the solution. Figure 1b shows the conductivity measured for NaClO_4 -based aqueous, organic, and mixed ($50:50$, v/v , $x_{\text{DMAc}} = 0.16$) electrolytes over a temperature range between 25 and 80°C . As expected, the conductivity is the highest for the aqueous media, reaching 111.4 mS cm^{-1} at 25°C . Under the same conditions, the binary electrolyte is characterized by a conductance equal to 38.9 mS cm^{-1} , which is much higher than for the pristine DMAc/ NaClO_4 mixture (12.24 mS cm^{-1}). In this respect, it exceeds the literature results obtained for the $\text{LiNO}_3/\text{H}_2\text{O}/\text{DMSO}$ binary system (17.28 mS cm^{-1}) [25], $\text{KOTF}/\text{H}_2\text{O}/\text{trimethyl phosphate}$ (up to ca. 17 mS cm^{-1}) [28], LiTFSI-based AWIS electrolytes (13.1 mS cm^{-1} , [22], 17.4 mS cm^{-1} [21]), and is similar to NaClO_4 -based WIS electrolyte (41.2 mS cm^{-1}) [27]. Different compositions of electrolytes were also tested, i.e., with DMAc concentrations of 70 and 80% (v/v) which corresponds to x_{DMAc} of 0.31 and 0.44 , respectively. The conductivity measured at 25°C , however, was equal to only 25.2 and 19.2 mS cm^{-1} . Since it was intended to design an electrolyte with enhanced safety and voltage window but without sacrificing much of the transport properties, it was reasonable to select a 50% (v/v) DMAc solution for further studies. Furthermore, the viscosity of such

electrolytes remains at a fairly low level (3.84 mP s vs. 6.79 mPa s for the DMAc electrolyte). Some of the physical parameters of the electrolytes measured at 25 °C are summarized in Table 2.

Table 2. Physicochemical properties of electrolytes.

Electrolyte	Conductivity (mS cm ⁻¹)	Viscosity (mPa s)	Density (g cm ⁻³)
H ₂ O/NaClO ₄	126.50	1.33	1.145
H ₂ O/DMAc/NaClO ₄	39.02	3.84	1.125
DMAc/NaClO ₄	12.24	6.79	1.087

It is also important to emphasize that no freezing of the hybrid electrolyte solution was observed by decreasing the temperature down to −30 °C (Figure 1c) which shows the potential applicability over a temperature range unreachable for aqueous capacitors. To diagnose flammability concerns, especially in the presence of perchlorates—a powerful oxidizing agent—attempts to determine the self-extinguishing time (SET) were made (Figure 1d). In general, SET (expressed in s g^{−1}) shows how long the sample burns after removing the ignition source. The pristine DMAc electrolyte ignites very easily and the average SET was high and equal to 164 s g^{−1}. On the contrary, the flammability of the mixed aqueous–organic sample was significantly reduced, i.e., no burning out of the sample was observed at all after the removal of the fire gun.

To provide additional quantitative information on how the electrolyte composition affects the electrode wettability, static contact angle measurements were performed using the AC pellet electrodes as a substrate for the electrolyte droplets. As seen in Figure 1e, the contact angle is the highest for an aqueous electrolyte (89.9°), while it is very similar for DMAc (60.2°) and a binary mixture (62.7°). It shows the beneficial effect of DMAc on the affinity of the electrolyte toward hydrophobic carbon, which is crucial for assuring facile ion diffusion inside highly microporous material during the capacitor's operation.

The high polarity of a carbonyl group present in the DMAc molecule enables the formation of H-bonds with water and other solvents, such as alcohols, where highly electronegative oxygen in the C=O acts as an H-bond acceptor [36–39]. In the case of DMAc, the phenomenon is additionally strengthened through the resonance effects characteristic of amides and by the presence of three methyl groups in the DMAc molecule. Furthermore, in the presence of a fairly concentrated perchlorate solution, changes in the ion-solvent interactions should be significant as well. The spectroscopic properties of H₂O, DMAc, and their mixture have been monitored here using FTIR (Figure 2a) and Raman spectroscopies (Figure 2b). The main bands that changed their positions, shape, or intensity, i.e., related to perchlorate anions [40–43] and the solvents [38,39,44], are marked in the spectra and enlarged in Figure S1. In the vibrational region of perchlorates (Raman spectra), the shift toward lower wavenumbers for the mixed solution (vs. pure H₂O) of the out-of-plane deformation band and symmetric stretching band of perchlorates (initially present at 627 and 933 cm^{−1}, respectively) is evident. The presence of the signal in the mixed electrolyte at a higher wavenumber than in the pristine DMAc (this trend is observable also in the FTIR spectra, Figure S1a) shows that salt is better dissociated in the mixed solvent solution and a lack of additional maxima in this region upon introduction of DMAc show that anions still interact with water molecules (through OH group) rather than with cations. Noteworthy, in the case of strong H₂O-cation association or H₂O-H₂O association in the mixed solvent, the intensity of the O-H signal at ca. 3250 cm^{−1} should be higher than for the pristine aqueous media. Therefore, the lower intensity (seen in Figure 2) suggests interactions of DMAc with H₂O.

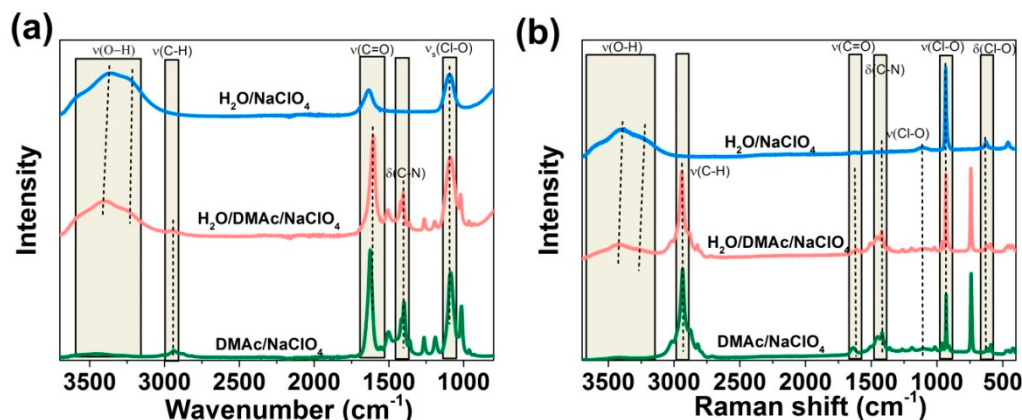


Figure 2. ATR-IR (a) and Raman spectra (b) of aqueous, organic, and hybrid electrolytes.

Indeed, the signal assigned to the stretching vibrations of carbonyl groups in DMAc ($\nu(\text{C}=\text{O})$) shows an apparent red-shift in the $\text{H}_2\text{O}/\text{DMAc}$ mixture from 1624 cm^{-1} in FTIR spectra (Figures 2a and S1a) which is also evident from Raman analysis (Figures 2b and S1b) and indicates the elongation and weakening of the bond. Having in mind that the $\text{C}=\text{O}$ signal is associated with both DMAc monomers and dimers (stabilized by weak $\text{C}=\text{O}\cdots\text{H}-\text{C}$ hydrogen bonds), the red-shift should be assigned to the weaker DMAc–DMAc interactions in the presence of water and salt [45]. In other words, weak $\text{C}-\text{H}\cdots\text{O}=\text{C}$ interactions are replaced by much stronger $\text{C}=\text{O}\cdots\text{H}-\text{O}$ but also $\text{C}=\text{O}\cdots\text{Na}^+$. The maximum of the $\nu(\text{C}=\text{O})$ in NaClO_4 –DMAc in the Raman spectra is located at 1638 cm^{-1} , while in the NaClO_4 –DMAc/ H_2O , with a closer look, the two bands can be distinguished—the stronger one at 1612 cm^{-1} and a shoulder at $\sim 1640 \text{ cm}^{-1}$. This indicates that in the mixed system, the interactions of the DMAc molecules involved in interactions both with cations and water are much stronger, than in the anhydrous one, although part of the DMAc appears to exist in the form of dimers. Another proof of this statement is the shift in both stretching and deformation bands related to C–N vibrations (see Figure S1a,b) towards higher wavenumber upon introducing H_2O , which shows further strengthening of the C–N bond and confirms the formation of both DMAc–cation and DMAc–water complexes.

A broad O–H stretching signal ($\nu(\text{O}-\text{H})$) seen at the highest wavenumbers corresponds to the different hydrogen bonding states of water [46]. Generally, in the presence of DMAc, the band shows a blue shift, which is especially pronounced for the maximum of the signal centered at 3364 cm^{-1} for a pure aqueous solution and 3396 cm^{-1} for the solvent mixture. This part of the band is assigned to the water molecules participating in the H-bond network, and a downshift shows the interactions between these H_2O molecules are weaker in the solvent mixture. Additionally, a blue shift appears in the binary mixture for the signal related to C–H stretching vibrations in methyl groups. Strengthening of this bond indicates interactions between methyl groups of DMAc and water, which can be ascribed to a weak H-bonding ($\text{C}-\text{H}\cdots\text{O}-\text{H}$) but also to charge redistribution due to the formation of $\text{C}=\text{O}\cdots\text{H}-\text{O}$ and $\text{C}=\text{O}\cdots\text{Na}^+$ [46,47]. In such a mixture, the mutual DMAc–DMAc interactions through $\text{C}=\text{O}$ and C–H groups are weakened, and fewer free water molecules are expected to be present in the system.

The H-bond formation is also evident from the thermal images recorded before and after the addition of DMAc to an aqueous solution of NaClO_4 (Figure 3a). Since no other chemical reactions occur in the mixed solution, the exothermic character of the process, seen as the rise in temperature up to 40°C upon mixing, should be attributed to the intermolecular H-bond interactions between water and DMAc. Additionally, as observed based on the ^{23}Na NMR spectra (Figure 3b), upon introduction of DMAc, the deshielding effect of the Na nucleus is evident as a downfield shift from -1.985 to -1.604 ppm . That confirms the spectroscopic results and indicates changes in the solvation structure of sodium in the electrolyte mixture, i.e., demonstrates that the organic constituent participates in the Na^+ solvation shell, which can be explained by its higher donor number ($27.8 \text{ kcal mol}^{-1}$

vs. 18.0 for H_2O). Similar findings were suggested for water/DMSO in the presence of sodium and zinc salts and very recently for water/DMAc/ZnSO₄ electrolyte of the Zn-ion battery [29,31,48].

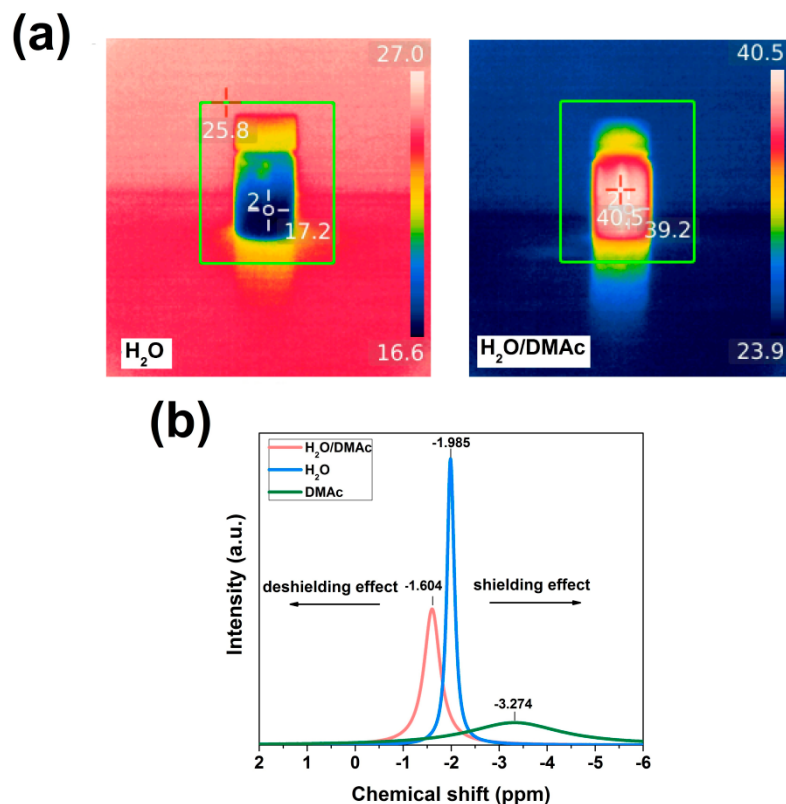


Figure 3. (a) Thermograms recorded with an infrared imaging camera showing a freshly prepared aqueous NaClO₄ solution before and after mixing with DMAc; (b) ^{23}Na NMR spectra of perchlorate salt in various solvents.

3.2. Electrochemical Properties of Electrolytes

The electrochemical stability window (ESW) of the hybrid electrolyte was evaluated at first using titanium electrodes (further used as current collectors of capacitors) under the linear sweep voltammetry (LSV) conditions and compared to the characteristics of the purely aqueous solution. Titanium was selected due to its chemical and electrochemical inertia and because a more economical alternative, i.e., the austenitic stainless steel current collectors, undergo corrosion in neutral salt electrolytes at elevated voltage [12,13]. As seen in Figure 4a, the expansion of the ESW in the $\text{H}_2\text{O}/\text{DMAc}$ electrolyte (compared to the aqueous counterpart) is seen in both the cathodic and anodic directions. In other words, suppression of both HER and OER is evident, allowing us to estimate the ESW on the level of 3.0 V (vs. 2.4 V for an aqueous system). It must be pointed out, however, that it does not reflect the practical voltage window of a capacitor using active carbon (AC) electrodes. In such a case, the hydrogen is stored in a porous carbon rather than released as a gas whilst the potential requirements of the positive AC electrode are largely limited to avoid its surface oxidation (corrosion).

Hence, the voltage windows were determined using AC as working electrodes of the three-electrode cells, and S-value analysis (Figure 4b) was conducted based on the cyclic voltammetry plots shown in Figure 4c,d. It allows for a straightforward evaluation of the minimum (E_{\min}) and maximum (E_{\max}) electrode potentials that can be reached by the electrodes to produce stable and reversible responses of a two-electrode system [49]. It is expressed as $S = Q_{\text{ch}}/Q_{\text{dch}} - 1$ where Q_{ch} and Q_{dch} correspond to the charges passing through the cell during the charge and discharge cycle, respectively. $S > 0.1$ typically

indicates the presence of 10% faradaic contributions, i.e., due to the electrolyte compositions. Judging from Figure 4a and further from Figure 4d (i.e., analyzing the region where the shape of the CV curves is close to rectangular), the ESW for the hybrid electrolyte-based capacitor is expected to approach 2.0 V. Such a wide ESW is due to the significantly suppressed HER potential in $\text{H}_2\text{O}/\text{DMAc}$ solution, i.e., it is far beyond the thermodynamic predictions described by the Pourboix diagram ($E_{\text{HER}} = -0.059 \text{ pH}$) for water for the solution with pH of 5–6. The suppression of HER is observed as much lower specific currents in the region of the lowest potentials (when compared to the aqueous system). Interestingly, the anodic branches of the CV profiles in the aqueous cell are similar to its aqueous–organic counterpart, and $S > 0.1$ is observed at a potential between 0.6–0.7 V. The S-value analysis, however, suggests a very narrow potential window in the cathodic region (i.e., limited to ca. -0.5 V), but that should be analyzed with caution as it is not related to the HER reaction but rather to a quasi-reversible hydrogen sorption/desorption processes in porous carbons [1]. In practice, the negative electrode of aqueous SIW-type systems can be safely polarized down to even lower potentials without H_2O decomposition to gaseous H_2 . Based on our experience and the CV profiles in Figure 4c, the ESW of an aqueous system was predicted as equal to ca. 1.5 V.

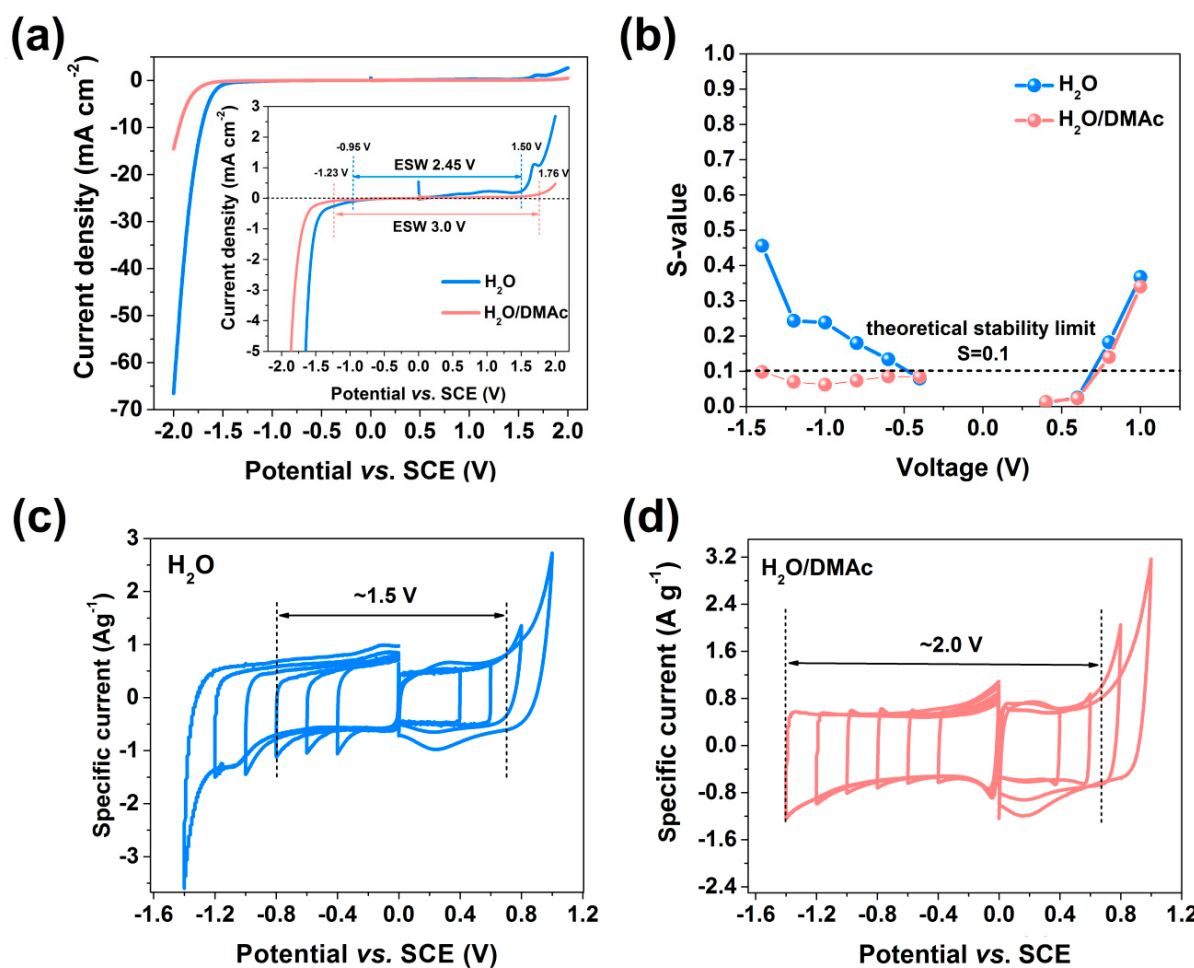


Figure 4. (a) Linear sweep voltammograms (LSV) illustrating the electrochemical stability window of aqueous, and aqueous–organic electrolytes using titanium electrodes. Inset shows the enlarged view on the LSV plot indicating onset potentials of solvent decomposition; (b) the evolution of S-value parameter vs. applied potential; (c,d) the cyclic voltammetry behavior observed for activated carbon electrodes in H_2O and $\text{H}_2\text{O}/\text{DMAc}$ electrolytes, respectively, in the three-electrode configuration. The scan rate: 0.005 V s^{-1} . The working AC electrode masses were equal to 5.17, and 5.31 mg for the cells with aqueous and aqueous–organic electrolytes, respectively.

One must keep in mind, however, that the realistic assessment of the maximum operating voltage can be deduced only by the detailed investigations of the two-electrode system, especially by exploring the practically observed potential windows of both electrodes vs. the reference electrode at the same time. For instance, in early studies, the capacitors with SIW electrolytes were reported to operate at 1.9 V [11]. Due to the complex aging processes, mainly related to the positive electrode and current collector corrosion processes, their safe and realistic potential window was found to be lower than initially expected and oscillated between 1.5 and 1.6 V [13,14]. Hence, both aqueous and aqueous–organic electrolytes were employed for the construction of the two-electrode symmetric cells (i.e., with an identical mass of the positive and negative electrode) whose voltage was successively expanded in 0.1 V steps. As seen in Figure 5, the CV characteristics of the cells (Figure 5a,c) as well as their electrodes (Figure 5b,d) do not show significant differences. The hybrid electrolyte-based system exhibits slightly higher coulombic efficiency at 1.7 V, which is due to slightly lower maximum currents characteristic for both electrodes at their fully charged state (see Figure 5b,d). These observations, however, reflect the discrete differences in the pH of electrolytes (Table 2) rather than some beneficial effect of a co-solvent. Figure 5e,f shows the evolution of the extreme electrode potentials for both systems upon voltage increase from 1.0 to 1.7 V.

Horizontal lines show the theoretically predicted HER and OER potentials at pH characteristics for both electrolytes. Please note that calculations were based on the real pH of the solutions, i.e., after exposure to AC electrodes, since the acid–base properties of carbon surfaces alter the neutral solution's pH. As seen, at the maximum applied voltage, both electrodes operate beyond the theoretical potential window of water regardless of the electrolyte. Although the negative electrodes are protected against gas evolution due to the high overpotential of HER in neutral media (as confirmed in Figure 4c,d), the operation at 1.7 V might be detrimental for the positive electrode. Indeed, the overpressure, ascribed to the formation of corrosion products (CO/CO₂) of the positive electrode, has been observed at elevated voltages in earlier studies with Li₂SO₄-based SIW electrolytes [12,13]. On the other hand, while the negative electrode of the aqueous system (Figure 5e) approaches its predicted (and “safe”) limit (see Figure 4c), its counterpart of the H₂O/DMAc system could be effectively polarized down to lower potentials of ca. –1.4 V (as shown in Figure 4d). However, it is impossible in a symmetric cell due to the limitation related to the positive electrode.

An appropriate cell design, i.e., employing mass asymmetry of electrodes, is a well-known strategy allowing the maximization of the operating cell voltage of capacitors [1,4]. Since the equalization of charges (Q) passing through the positive (Q_+) and negative (Q_-) electrodes is a fundamental requirement for each electrochemical cell (1) and by taking into account the definition of mass-normalized (m) capacitance (C) (2), the law of conservation of charge can be expressed as (3):

$$Q_+ = Q_- \quad (1)$$

$$C = \frac{Q}{Um} \quad (2)$$

$$C_+ \Delta E_+ m_+ = C_- \Delta E_- m_- \quad (3)$$

where C_+/C_- , $\Delta E_+/\Delta E_-$, and m_+/m_- are the capacitance, potential range, and mass of the positive and negative electrodes, respectively. It is clear then that to widen the potential window of the negative electrode of the H₂O/DMAc system, the mass-oversized positive electrode should be employed for the construction of the cell. Based on the theoretical calculations using data in Figure 4b–d, as well as on the experimental trials using different m_+/m_- ratios ranging from 1.26 to 2.83, the best adjustments of the electrode potential ranges were obtained for $m_+/m_- = 1.51$. As can be seen in Figure 6a, which shows the potential ranges of the individual electrodes as a function of voltage, the extreme potentials reached by the positive and the negative electrodes at 2.0 V are now equal to 0.57 and –1.43 V vs. 0.72 and –0.98 V for symmetric cell with a hybrid electrolyte (Figure 5f). It

allows the operation of the positive electrode in a more “safe” potential range, i.e., below the OER region, thus protecting it from electrochemical aging. On the other hand, the opposite electrode can fully use the benefits of a hybrid electrolyte, i.e., the regulated solvent structure and suppression of HER. Figure 6b shows the CV responses of a capacitor at a different voltage, and as seen, almost ideal rectangular-like CVs were obtainable up to 2.0 V. At more extensive polarization, distortion in current-voltage dependencies appeared, thus suggesting overcharge that would result in faster aging. Figure 6c shows the GCD characteristics at different charge–discharge currents applied to the cell, including contributions from the individual electrodes, and confirming the rational design of the asymmetric system predicted by applying voltammetric conditions (Figure 6a).

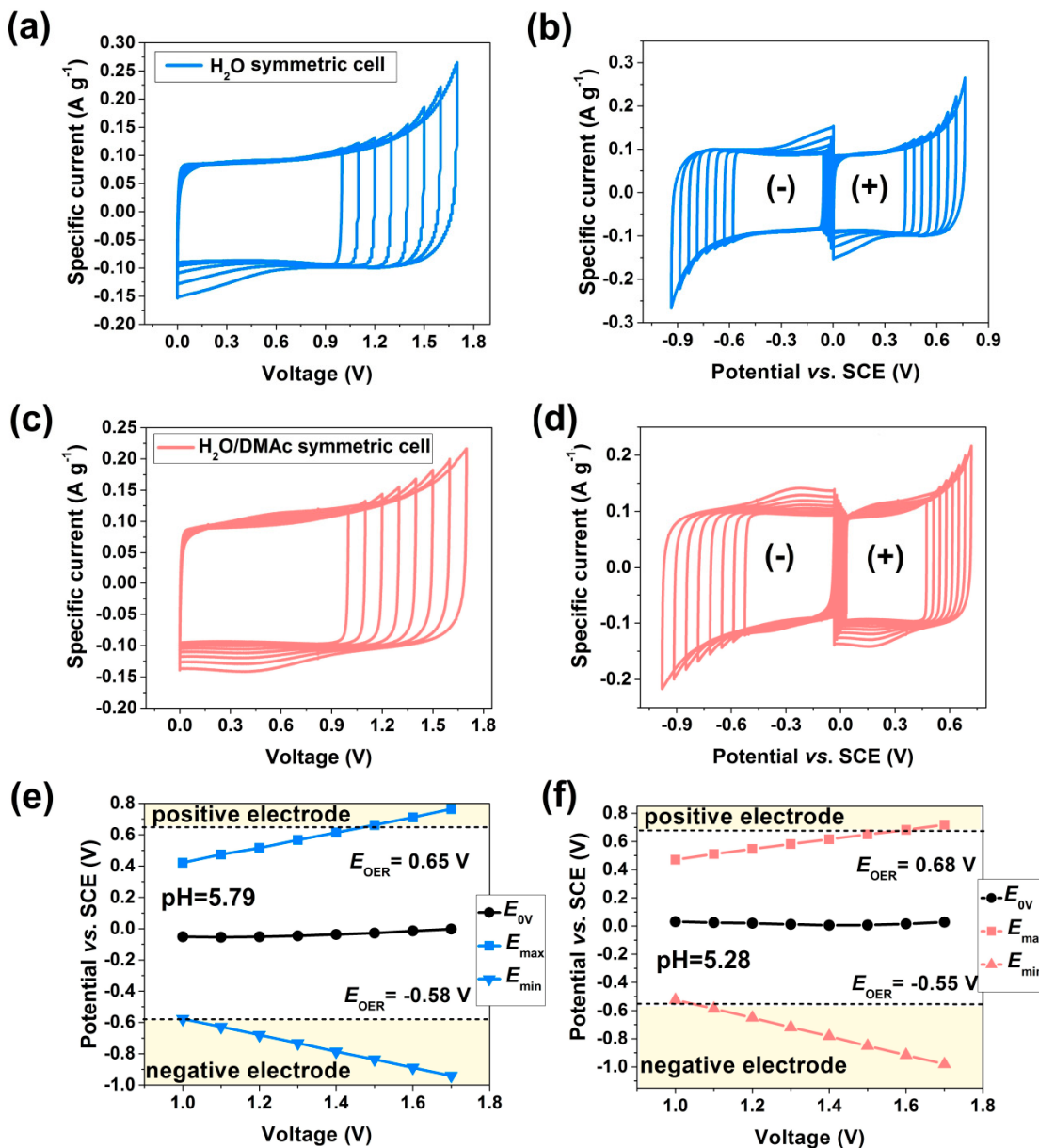


Figure 5. (a,c) Cyclic voltammetry characteristics of the symmetric H_2O ($m_+ = 5.61 \text{ mg}$, $m_- = 5.91 \text{ mg}$), and $\text{H}_2\text{O}/\text{DMAc}$ -based capacitors ($m_+ = 5.77 \text{ mg}$, $m_- = 5.79 \text{ mg}$), respectively, recorded at different cell voltages along with corresponding potential ranges of the individual (the positive and negative) electrodes (b,d) as well as the extreme potential values reached by both electrodes at a given voltage (e,f). Horizontal dash lines in (e,f) illustrate the theoretical onset of HER and OER at pH characteristics for both electrolytes exposed to AC. The scan rate was equal to 0.005 V s^{-1} .

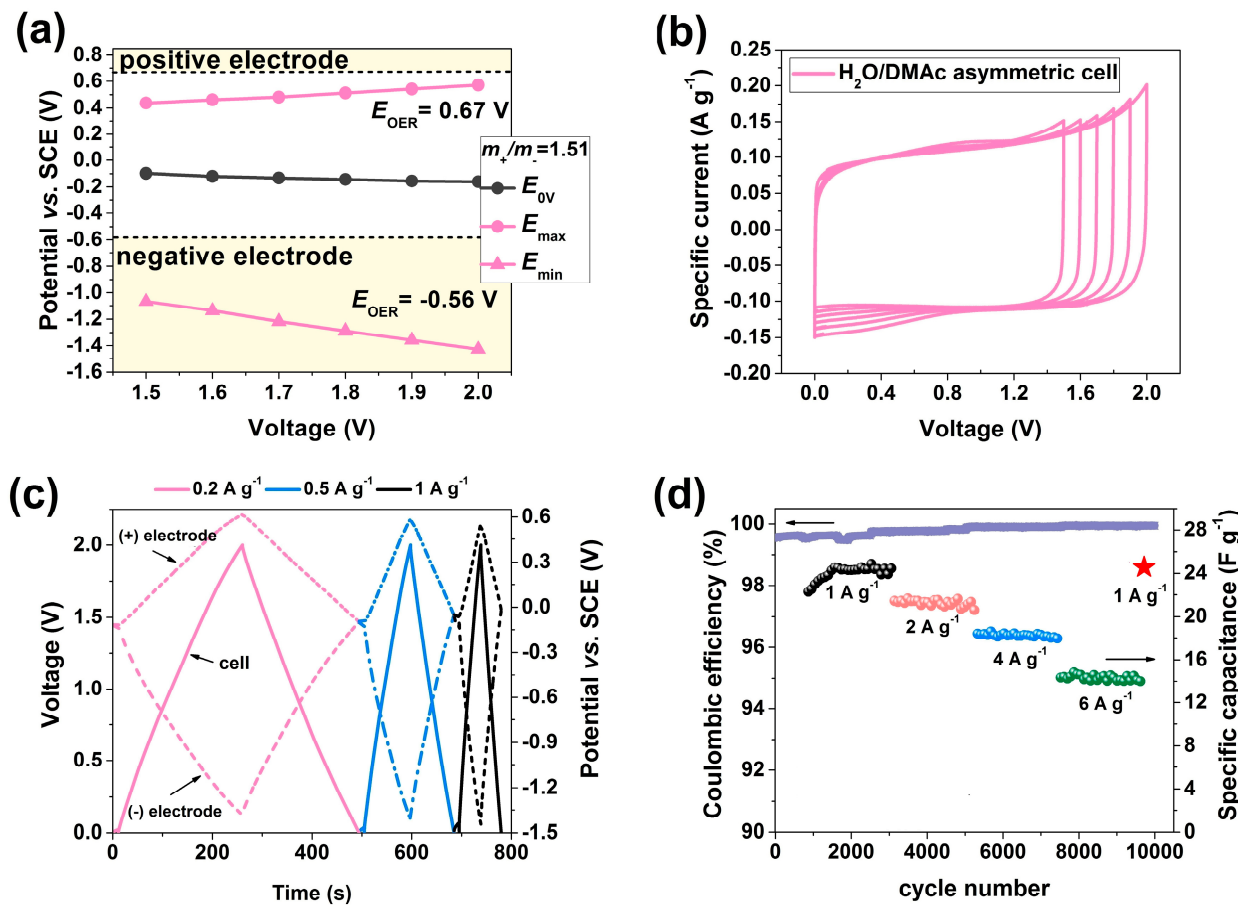


Figure 6. (a) Potential ranges of the individual electrodes of the asymmetric $\text{H}_2\text{O}/\text{DMAc}$ capacitors as a function of voltage; (b) cyclic voltammetry curves of the asymmetric system (0.005 V s^{-1}); (c) GCD characteristics of the 2.0 V asymmetric cell along with the simultaneously monitored potential windows of the positive and negative electrodes at different specific currents; (d) Cyclic performance of the 2.0 V system at different charge–discharge currents. m_+/m_- ratio was equal to 1.51 ($m_+ = 5.55 \text{ mg}$, $m_- = 3.67 \text{ mg}$).

The cyclic performance involving four series of 2,500 GCD cycles at progressively increasing specific currents is presented in Figure 6d. Under applied conditions, after the initial rise in the capacitance, which might be assigned to stabilization of the electrochemical response due to the ion arrangement in pores of the AC (electrode wetting), the system fully retained its charge–discharge properties whilst the coulombic efficiency approached 100% through the whole test period. The red star symbol shows the capacitance measured after the accomplishment of the cycling procedure, while Figure S2 shows the EIS Nyquist plots recorded before the first GCD cycle and after the whole procedure. It is noteworthy that the overall resistance, taken as a sum of solution and charge transfer contributions, increased from 2.1 to 3.1Ω . Meanwhile, the end-of-life of electrochemical capacitors is often associated with their capacitance decrease by 20% and a two-fold increase in the series resistance [50,51]. Hence, the results show the cell did not reach the end-of-life after 10,000 cycles. As mentioned earlier, at voltage $>2.0 \text{ V}$, the asymmetric cell with a hybrid electrode revealed signs of instability. In the course of the study, the cyclability test was also performed at 2.2 V at a specific current of 1 A g^{-1} . The capacitance retention was equal to 83%, suggesting an overcharge. The pH of the aged electrolyte measured with an indicator was equal to ca. 3, which is presumably related to excessive oxidation of the positive electrode upon continuous cycling to CO and finally to CO_2 . Therefore, it is reasonable to expect that the maximum voltage of this particular system cannot be extended above 2.0 V .

The asymmetric H₂O/DMAc system was subjected to electrochemical testing at different temperatures to obtain more insight into the rate performance. Figure 7a shows the CV curves at low ($-20, 0$ °C), elevated (60 °C), and room temperature (RT). The results are shown for the scan rate of 0.05 V s $^{-1}$ to allow easier analysis of distortions of the CV due to the rise in the resistance contributions. Changes in the slope of the CV curve at the beginning of the charge and discharge cycle reflect a rise in the internal resistance due to temperature-dependent properties of the electrolyte, i.e., ionic conductivity decreased (e.g., from 80.4 mS cm $^{-1}$ at 60 °C to 5.2 mS cm $^{-1}$ at 0 °C) and viscosity increased (from 1.87 to 4.37 mPa s, respectively) with decreasing temperature. An excellent capacitive behavior was, however, observed at temperatures as low as at least 0 °C. Figure 7b shows the Ragone plots for all investigated systems derived from the GCD measurements at specific currents ranging from 0.1 to 10 A g $^{-1}$ (some examples of the GCD curves recorded at different temperatures are shown in Figure S3). The maximum specific energy for the systems measured at 0.1 A g $^{-1}$ was equal to $17.7, 13.2, 12.8$, and 12.1 Wh kg $^{-1}$ at 60 , RT, 0 , and -20 °C and uniformly decreased for all systems up to the current of 1 A g $^{-1}$ which shows that at least at low to moderate current densities, the H₂O/DMAc system's performance was at a reasonable level over the whole range of temperatures. At higher discharge currents, the capacitor's responses reflected the aforementioned deterioration in the physical properties of electrolytes, which is observed as the energy fades at high specific power. Nevertheless, the energy of 12.3 (60 °C), 10.8 (RT), 7.9 (0 °C), and 1.0 Wh kg $^{-1}$ (-20 °C) was still available at the specific power of 2 kW kg $^{-1}$ which demonstrates the practical significance of the system for applications in a wide spectrum of environmental conditions.

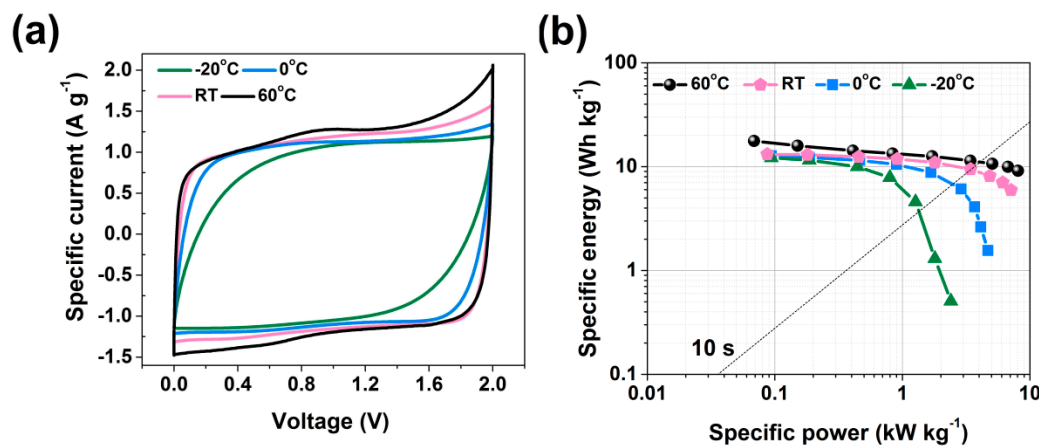


Figure 7. (a) Cyclic voltammetry characteristics (scan rate of 0.05 V s $^{-1}$) and (b) the Ragone plots of asymmetric systems with a hybrid electrolyte tested at different temperatures.

The question that arises is about the advantages and limitations of the hybrid electrolyte-based system in comparison to its aqueous counterpart. A natural consequence of voltage enhancement is an increase in energy. The unknown issue is, however, whether and how the limited conductivity and elevated viscosity of an aqueous–organic electrolyte influence the rate performance of the system. Figure 8a shows the Ragone plots for an optimized hybrid electrolyte-based system operating at 2.0 V and an aqueous counterpart operating at 1.5 V, i.e., reported as a stable voltage of the SIW electrolyte systems [13,14]. The maximum specific energy derived from the GCD tests was equal to 7.5 and 13.2 Wh kg $^{-1}$ for H₂O, and H₂O/DMAc-based capacitors, which means a significant rise of 76% upon introducing an organic solvent, and that is directly assigned to the increase in the operating voltage. Additionally, within 10 s (marked in Figure 8a), the system with a hybrid electrolyte was able to deliver 9.5 Wh kg $^{-1}$ with a power of 3.4 kW kg $^{-1}$ whilst it was only 6.9 Wh kg $^{-1}$ at 2.4 kW kg $^{-1}$ for the aqueous counterpart. The highest specific capacitance, i.e., determined at 0.1 A g $^{-1}$, was, however, almost identical, i.e., equal to 24.5 and 24.0 F g $^{-1}$ for H₂O and H₂O/DMAc, thus, showing similar charge storage properties at low discharge rates.

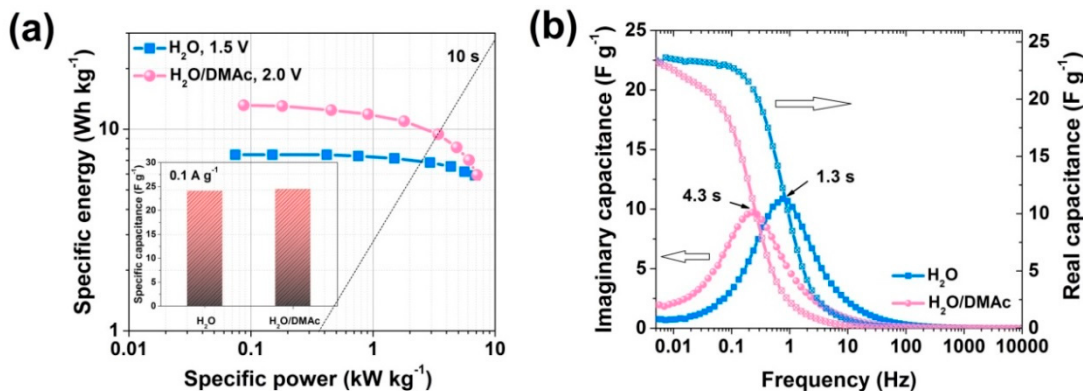


Figure 8. (a) The Ragone plots (with the inset including the specific capacitance determined at 0.1 A g^{-1}), and (b) the real and imaginary complex capacitance plotted vs. frequency for the symmetric aqueous ($m_+ = 5.67 \text{ mg}$, $m_- = 5.72 \text{ mg}$) and asymmetric aqueous–organic ($m_+ = 3.74 \text{ mg}$, $m_- = 5.65 \text{ mg}$) capacitors.

Based on the EIS Nyquist plots, the imaginary and real components of a complex capacitance were derived and plotted as a function of frequency (Figure 8b) [52]. Such results show how the resistance contributions, which, due to the physical properties of the electrolyte, were larger in the case of the H₂O/DMAc system, influence the rate performance. For instance, from the plot of the real capacitance component vs. frequency, it can be seen that at the frequency of 1 Hz, the capacitance of 9.7 and 2.3 F g^{-1} was found for aqueous and aqueous–organic systems, respectively. It demonstrates that a charge–discharge process was less complete at higher rates in the case of the H₂O/DMAc capacitor. Additionally, the relaxation time constant determined from the maximum of the peak signal on the plot of the imaginary component of capacitance vs. frequency as $\tau = 1/f_0$ was higher for the H₂O/DMAc system (4.3 s vs. 1.3 s for an aqueous cell). The time constant reflects the boundary conditions between capacitive and resistive behavior. Since all cell parameters that might influence the τ parameter, i.e., type and thickness or electrodes/separators, and assembly conditions were identical, the differences are solely associated with charge–discharge rates in a given electrolyte. Realistically speaking then, the charge propagation in storage is sacrificed upon the addition of the organic solvent, but the system still benefits a lot from the improved energy, which is maintained even at higher discharge rates. To the best of our knowledge, such a realistic assessment is demonstrated for the first time, thus, showing a trade between energy and power capabilities. For this reason, care must be taken when designing hybrid electrolytes to keep the rate capabilities, the main advantage of electrochemical capacitors, at a reasonable level.

Comparing the performance of the developed system to other voltage-enhancement strategies existing in the literature, the obtained specific energy of 11.8 Wh kg^{-1} (at 1 kW kg^{-1}) was higher than for the 2.2 V system utilizing choline chloride/urea deep eutectic solvent as electrolyte (7.0 Wh kg^{-1}) [53], 1.8 V capacitor based on H₂O/DMSO/NaNO₃ solution (4.5 Wh kg^{-1}) [25], and 2.0 V H₂O/DMSO/redox active polyoxometallate-based system (9.0 Wh kg^{-1}) [25]. The specific energy extracted from the GCD data at 1 A g^{-1} also exceeds the performance of a 3.0 V ionic liquid (EMIImBF₄)-based capacitor (1.79 Wh kg^{-1}), which was greatly affected by the low ionic conductivity of the solution [54]. However, one must be aware that such a comparison does not take into account the differences in the fabrication procedures, i.e., even the same system using electrodes that vary in thickness and mass loading or are tested in different measurement cells that may give different results. The type of carbon material and its porosity affect the maximum parameters and rate performance as well. Therefore, caution should be taken when generalizing the results.

4. Conclusions

This work highlights the beneficial properties of hybrid aqueous–organic electrolytes based on water/N,N-dimethylacetamide (DMAc) solvent mixtures for applications in electrochemical energy storage devices such as electrochemical capacitors but relevant also for battery research. Compared with organic systems, the enhanced safety, due to the flame-retardant properties, and relatively low cost, by introducing sodium perchlorate instead of expensive lithium salts or those with large quaternary ammonium cations limiting the ionic transport, should be underlined at first. Improved wettability of the electrode/electrolyte interface (when compared with aqueous media) is of significant importance in providing facile ion diffusion in carbon pores despite lower conductivity (vs. aqueous counterpart).

Importantly, the formation of strong hydrogen bonds between H₂O (H-bond donor) and DMAc (H-bond acceptor) in an electrolyte mixture, along with the participation of DMAc in Na⁺ solvation shell, was found to suppress the water electrolysis. As a result, even for the electrolytes with a fairly low mole fraction of DMAc, intentionally fixed at 0.16, the electrochemical stability window of the electrolyte reaches 3.0 V at bare titanium electrodes. The operating voltage of a capacitor based on the carbonaceous electrodes must be, however, carefully correlated with the electrochemical stability of the positive electrode to avoid its electrochemical degradation (oxidation). Nevertheless, upon appropriate mass balancing ($m_+/m_- = 1.51$), the system with a binary electrolyte still benefits from the suppressed HER potential by ca. 0.5 V, which gives the rise in the operating cell voltage up to 2.0 V and, consequently, the energy density, while maintaining excellent cyclic stability and decent performance at temperatures down to $-20\text{ }^{\circ}\text{C}$.

Even at high discharge rates (exemplified for 10 s discharge time at RT), the system delivers 9.5 Wh kg⁻¹ with a power of 3.4 kW kg⁻¹ (vs. 6.9 Wh kg⁻¹ at 2.4 kW kg⁻¹ for the aqueous counterpart operating at 1.5 V). To conclude, the system benefits from both the physical properties of the individual components and also from the synergistic effect related to the mutual intermolecular interactions. In this regard, it fills the gap between aqueous and organic system performances.

Supplementary Materials: The following supporting information can be downloaded at: <https://www.mdpi.com/article/10.3390/batteries10060213/s1>, Figure S1: Enlarged view on (a) ATR-IR and (b) Raman spectra of electrolytes showing changes in the positions of characteristic bands., Figure S2: The EIS Nyquist plots recorded for the asymmetric capacitor with a hybrid H₂O/DMAc electrolyte before and after 10,000 charge-discharge cycles., Figure S3: The GCD characteristic of the asymmetric capacitor with a hybrid H₂O/DMAc electrolyte at different temperatures.

Author Contributions: Conceptualization, M.S.-N.; methodology, A.A.M. and M.S.-N.; validation, G.Z.Ż. and M.S.-N.; formal analysis, K.S., G.Z.Ż. and M.S.-N.; investigation, A.A.M., K.S. and G.Z.Ż.; resources, M.S.-N.; data curation, A.A.M., K.S. and G.Z.Ż.; writing—original draft preparation, M.S.-N.; writing—review and editing, M.S.-N.; visualization, K.S.; and M.S.-N.; supervision, M.S.-N.; project administration, M.S.-N.; funding acquisition, M.S.-N. and A.A.M. All authors have read and agreed to the published version of the manuscript.

Funding: This work was financially supported by the National Science Centre (grant MINIATURA 6 no. 2022/06/X/ST4/00136) and in part by the University of Warsaw in the framework of the “Excellence Initiative–Research University Programme of the Ministry of Science and Higher Education under student grant no IDUB-622-698/2023 (Action IV.4.1).

Data Availability Statement: The original contributions presented in the study are included in the article, further inquiries can be directed to the corresponding author.

Acknowledgments: The authors also would like to acknowledge Imerys Graphite and Carbon and Kuraray, for supplying carbon black and activated carbon powders, respectively.

Conflicts of Interest: The authors declare no conflict of interest.

References

1. Beguin, F.; Presser, V.; Balducci, A.; Frackowiak, E. Carbons and electrolytes for advanced supercapacitors. *Adv. Mater.* **2014**, *26*, 2219–2251. [[CrossRef](#)]
2. Wang, Y.; Song, Y.; Xia, Y. Electrochemical capacitors: Mechanism, materials, systems, characterization and applications. *Chem. Soc. Rev.* **2016**, *45*, 5925–5950. [[CrossRef](#)]
3. Pal, B.; Yang, S.; Ramesh, S.; Thangadurai, V.; Jose, R. Electrolyte selection for supercapacitive devices: A critical review. *Nanoscale Adv.* **2019**, *1*, 3807–3835. [[CrossRef](#)]
4. Pineiro-Prado, I.; Salinas-Torres, D.; Ruiz-Rosas, R.; Morallon, E.; Cazorla-Amoros, D. Design of activated carbon/activated carbon asymmetric capacitors. *Front. Mater.* **2016**, *3*, 1–12. [[CrossRef](#)]
5. Miao, L.; Song, Z.; Zhu, D.; Li, L.; Gan, L.; Liu, M. Ionic liquids for supercapacitive energy storage: A mini-review. *Energ. Fuel.* **2021**, *35*, 8443–8455. [[CrossRef](#)]
6. Salanne, M. Ionic liquids for supercapacitor applications. *Top Curr. Chem.* **2017**, *375*, 1–25. [[CrossRef](#)]
7. Puttaswamy, R.; Mondal, C.; Mondal, D.; Ghosh, D. An account on the deep eutectic solvents-based electrolytes for rechargeable batteries and supercapacitors. *Sustain. Mater. Technol.* **2022**, *33*, e00477. [[CrossRef](#)]
8. Ruiz, V.; Santamaría, R.; Granda, M.; Blanco, C. Long-term cycling of carbon-based supercapacitors in aqueous media. *Electrochim. Acta* **2009**, *54*, 4481–4486. [[CrossRef](#)]
9. Demarconnay, L.; Raymundo-Pinero, E.; Beguin, F. A symmetric carbon/carbon supercapacitor operating at 1.6 V by using a neutral aqueous solution. *Electrochem. Commun.* **2010**, *12*, 1275–1278. [[CrossRef](#)]
10. Bichat, M.P.; Raymundo-Pinero, E.; Beguin, F. High voltage supercapacitor built with seaweed carbons in neutral aqueous electrolyte. *Carbon* **2010**, *48*, 4351–4361. [[CrossRef](#)]
11. Gao, Q.; Demarconnay, L.; Raymundo-Pinero, E.; Beguin, F. Exploring the large voltage range of carbon/carbon supercapacitors in aqueous lithium sulfate electrolyte. *Energy Environ. Sci.* **2012**, *5*, 9611–9617. [[CrossRef](#)]
12. Ratajczak, P.; Jurewicz, K.; Beguin, F. Factors contributing to ageing of high voltage carbon/carbon supercapacitors in salt aqueous electrolyte. *J. Appl. Electrochem.* **2014**, *44*, 475–480. [[CrossRef](#)]
13. Ratajczak, P.; Jurewicz, K.; Skowron, P.; Abbas, Q.; Beguin, F. Effect of accelerated ageing on the performance of high voltage carbon/carbon electrochemical capacitors in salt aqueous electrolyte. *Electrochim. Acta* **2014**, *130*, 344–350. [[CrossRef](#)]
14. Abbas, Q.; Beguin, F. High voltage AC/AC electrochemical capacitor operating at low temperature in salt aqueous electrolyte. *J. Power Sources* **2016**, *318*, 235e241. [[CrossRef](#)]
15. Suo, L.; Borodin, O.; Gao, T.; Olguin, M.; Ho, J.; Fan, X.; Luo, C.; Wang, C.; Xu, K. “Water-in-salt” electrolyte enables high-voltage aqueous lithium-ion chemistries. *Science* **2015**, *350*, 938–943. [[CrossRef](#)]
16. Bu, X.; Su, L.; Dou, Q.; Lei, S.; Yan, X. A low-cost “water-in-salt” electrolyte for a 2.3 V high-rate carbon-based supercapacitor. *J. Mater. Chem. A* **2019**, *7*, 7541–7547. [[CrossRef](#)]
17. Tian, X.; Zhu, Q.; Xu, B. “Water-in-Salt” electrolytes for supercapacitors: A review. *ChemSusChem* **2021**, *14*, 2501–2515. [[CrossRef](#)]
18. Pang, M.; Jiang, S.; Zhao, J.; Zhang, S.; Wang, R.; Li, N.; Liu, R.; Pan, Q.; Qu, W.; Xing, B. “Water-in-salt” electrolyte enhanced high voltage aqueous supercapacitor with carbon electrodes derived from biomass waste-ground grain hulls. *RSC Adv.* **2020**, *10*, 35545. [[CrossRef](#)]
19. Lannelongue, P.; Bouchal, R.; Mourad, E.; Bodin, C.; Olarte, M.; le Vot, S.; Favier, F.; Fontaine, O. “Water-in-Salt” for supercapacitors: A compromise between voltage, power density, energy density and stability. *J. Electrochem. Soc.* **2018**, *165*, A657–A663. [[CrossRef](#)]
20. Park, J.; Lee, J.; Kim, W. Water-in-Salt Electrolyte enables ultrafast supercapacitors for AC line filtering. *ACS Energy Lett.* **2021**, *6*, 769–777. [[CrossRef](#)]
21. Dou, Q.; Lei, S.; Wang, D.-W.; Zhang, Q.; Xiao, D.; Guo, H.; Wang, A.; Yang, H.; Li, Y.; Shi, S.; et al. Safe and high-rate supercapacitors based on an “acetonitrile/water in salt” hybrid electrolyte. *Energy Environ. Sci.* **2018**, *11*, 3212–3219. [[CrossRef](#)]
22. Xiao, D.; Dou, Q.; Zhang, L.; Ma, Y.; Shi, S.; Lei, S.; Yu, H.; Yan, X. Optimization of organic/water hybrid electrolytes for high-rate carbon-based supercapacitor. *Adv. Funct. Mater.* **2019**, *29*, 1904136. [[CrossRef](#)]
23. Ye, W.; Wang, H.; Ning, J.; Zhong, Y.; Hu, Y. New types of hybrid electrolytes for supercapacitors. *J. Energy Chem.* **2021**, *57*, 219–232. [[CrossRef](#)]
24. Khosrozadeh, A.; Tao, L.; Zhao, P.; Miller, M.B.; Voznyy, O.; Liu, J. Water/acetonitrile hybrid electrolyte enables using smaller ions for achieving superior energy density in carbon-based supercapacitors. *J. Power Sources* **2021**, *498*, 229905. [[CrossRef](#)]
25. Dsoke, S.; Abbas, Q. Benefits of organo-aqueous binary solvents for redox supercapacitors based on polyoxometalates. *ChemElectroChem* **2020**, *7*, 2466–2476. [[CrossRef](#)]
26. Wang, H.; Deng, Y.; Qiu, J.; Wu, J.; Zhang, K.; Shao, J.; Yan, L. In situ formation of “Dimethyl Sulfoxide/Water-in-Salt”-based chitosan hydrogel electrolyte for advanced all-solid-state supercapacitors. *ChemSusChem* **2021**, *14*, 632–641. [[CrossRef](#)]
27. Dou, Q.; Lu, Y.; Su, L.; Zhang, X.; Lei, S.; Bu, X.; Liu, L.; Xiao, D.; Chen, J.; Shi, S.; et al. A sodium perchlorate-based hybrid electrolyte with high salt-to-water molar ratio for safe 2.5 V carbon-based supercapacitor. *Energy Storage Mater.* **2019**, *23*, 603–609. [[CrossRef](#)]
28. Wu, S.; Su, B.; Sun, M.; Gu, S.; Lu, Z.; Zhang, K.; Yu, D.Y.W.; Huang, B.; Wang, P.; Lee, C.-S.; et al. Dilute aqueous-aprotic hybrid electrolyte enabling a wide electrochemical window through solvation structure engineering. *Adv. Mater.* **2021**, *33*, 2102390. [[CrossRef](#)]

29. Nian, Q.; Zhang, X.; Feng, Y.; Liu, S.; Sun, T.; Zheng, S.; Ren, X.; Tao, Z.; Zhang, D.; Chen, J. Designing electrolyte structure to suppress hydrogen evolution reaction in aqueous batteries. *ACS Energy Lett.* **2021**, *6*, 2174–2180. [CrossRef]
30. Wang, L.; Uosaki, K.; Noguchi, H. Effect of electrolyte concentration on the solvation structure of gold/LITFSI–DMSO Solution Interface. *J. Phys. Chem. C* **2020**, *124*, 12381–12389. [CrossRef]
31. Cao, L.; Li, D.; Hu, E.; Xu, J.; Deng, T.; Ma, L.; Wang, Y.; Yang, X.-Q.; Wang, C. Solvation structure design for aqueous Zn metal batteries. *J. Am. Chem. Soc.* **2020**, *142*, 21404–21409. [CrossRef]
32. National Center for Biotechnology Information (2024). PubChem Compound Summary for CID 31374, N,N-Dimethylacetamide. Available online: <https://pubchem.ncbi.nlm.nih.gov/compound/N,N-Dimethylacetamide> (accessed on 12 June 2024).
33. National Center for Biotechnology Information (2024). PubChem Compound Summary for CID 6342, Acetonitrile. Available online: <https://pubchem.ncbi.nlm.nih.gov/compound/Acetonitrile> (accessed on 12 June 2024).
34. Wohlfahrt, C. Static dielectric constants of pure Liquids and binary liquid mixtures. In *Landolt-Börnstein: Numerical Data and Functional Relationships in Science and Technology—New Series*, IV/17; Lechner, M.D., Ed.; Springer Science & Business Media: Berlin/Heidelberg, Germany, 2008. [CrossRef]
35. Zhong, C.; Deng, Y.; Hu, W.; Qiao, J.; Zhang, L.; Zhang, J. A review of electrolyte materials and compositions for electrochemical supercapacitors. *Chem. Soc. Rev.* **2015**, *44*, 7484–7539. [CrossRef]
36. Zaichikov, A.M.; Bushuev, Y.G. The thermodynamic properties of the water-dimethylacetamide system. *Russ. J. Phys. Chem.* **1995**, *69*, 1766–1770.
37. Manjunath, M.S.; Sivagurunathan, P.; Sannappa, J. Studies of hydrogen bonding between N, N-Dimethylacetamide and primary alcohols. *E-J. Chem.* **2009**, *6*, 120362m. [CrossRef]
38. Schmid, E.; Brodbek, E. Raman intensity calculations with the CNDO method. Part 111: N,N-dimethylamide-water complexes. *Can. J. Chem.* **1985**, *63*, 1365–1371. [CrossRef]
39. Durgaprasad, G.; Sathyaranayana, D.N.; Patel, C.C.; Randhawa, H.S.; Goel, A.; Rao, C.N.R. Normal vibrations of N,N-dimethylacetamide. *Spectrochim. Acta Part A Mol. Spectrosc.* **1972**, *28*, 2311–2318. [CrossRef]
40. Qu, H.; Ling, Z.; Qi, X.; Xin, Y.; Liu, C.; Cao, H. A remote Raman system and its applications for planetary material studies. *Sensors* **2021**, *21*, 6973. [CrossRef]
41. Chen, Y.; Zhang, Y.-H.; Zhao, L.-J. ATR-FTIR spectroscopic studies on aqueous LiClO₄, NaClO₄, and Mg(ClO₄)₂ solutions. *Phys. Chem. Chem. Phys.* **2004**, *6*, 537–542. [CrossRef]
42. Cvjeticanin, N.D.; Sasic, S. Raman spectroscopic study of lithium and sodium perchlorate association in propylene carbonate–water mixed solvents. *J. Raman Spectrosc.* **2000**, *31*, 871–876. [CrossRef]
43. Chabanel, M.; Legoff, D.; Touaj, K. Aggregation of perchlorates in aprotic donor solvents. Part 1.—Lithium and sodium perchlorates. *J. Chem. Soc. Faraday Trans.* **1996**, *92*, 4199–4205. [CrossRef]
44. Chalapathi, V.V.; Ramiah, K.V. Normal vibrations of N, N-dimethylformamide and N, N-dimethylacetamide. *Proc. Ind. Acad. Sci.* **1968**, *68*, 109. [CrossRef]
45. Kotov, N.; Raus, V.; Dybal, J. Intermolecular interactions in N, N-dimethylacetamide without and with LiCl studied by infrared spectroscopy and quantum chemical model calculations. *J. Phys. Chem. B.* **2018**, *122*, 8921–8930. [CrossRef]
46. Yang, B.; Cao, X.; Wang, C.; Wang, S.; Sun, C. Investigation of hydrogen bonding in Water/DMSO binary mixtures by Raman spectroscopy. *Spectrochim. Acta* **2020**, *228*, 117704. [CrossRef]
47. Wallace, V.M.; Dhumal, N.R.; Zehentbauer, F.M.; Kim, H.J.; Kiefer, J. Revisiting the aqueous solutions of dimethyl sulfoxide by spectroscopy in the mid- and near-infrared: Experiments and CarParrinello simulations. *J. Phys. Chem. B* **2015**, *119*, 14780–14789. [CrossRef]
48. Li, M.; Feng, X.; Yin, J.; Cui, T.; Li, F.; Chen, J.; Lin, Y.; Xu, X.; Ding, S.; Wang, J. Regulating the solvation structure with N,N-dimethylacetamide co-solvent for high-performance zinc-ion batteries. *J. Mater. Chem. A* **2023**, *11*, 2554. [CrossRef]
49. Weingarth, D.; Noh, H.; Foelske-Schmitz, A.; Wokaun, A.; Kötz, R. A reliable determination method of stability limits for electrochemical, double layer capacitors. *Electrochim. Acta* **2013**, *103*, 119–124. [CrossRef]
50. Oukaour, A.; Tala-Ighil, B.; AlSakka, M.; Gualous, H.; Gallay, R.; Boudart, B. Calendar ageing and health diagnosis of supercapacitor. *Elec. Power. Sys. Res.* **2013**, *95*, 330–338. [CrossRef]
51. Piwek, J.; Platek-Mielczarek, A.; Frackowiak, E.; Fic, K. Enhancing capacitor lifetime by alternate constant polarization. *J. Power Sources* **2021**, *506*, 230131. [CrossRef]
52. Taberna, P.L.; Simon, P.; Fauvarque, J.F. Electrochemical characteristics and impedance spectroscopy studies of carbon-carbon supercapacitors. *J. Electrochem. Soc.* **2003**, *150*, A292e–A300. [CrossRef]
53. Azmi, S.; Koudahia, M.F.; Frackowiak, E. Reline deep eutectic solvent as a green electrolyte for electrochemical energy storage applications. *Energy Environ. Sci.* **2022**, *15*, 1156–1171. [CrossRef]
54. Tee, E.; Tallo, I.; Thomberg, T.; Janes, A.; Lust, E. Supercapacitors Based on Activated Silicon Carbide-Derived Carbon Materials and Ionic Liquid. *J. Electrochem. Soc.* **2016**, *163*, A131.